ELSEVIER

Contents lists available at ScienceDirect

# Ceramics International

journal homepage: www.elsevier.com/locate/ceramint



# Counterions present in syntheses induce the precipitation of two different populations of Sr-containing hydroxyapatite crystals



L.M. Silva<sup>a</sup>, D.S. Menezes<sup>a</sup>, S. Narayanan<sup>b</sup>, T. Shokuhfar<sup>b</sup>, R. Shahbazian-Yassar<sup>b</sup>, G.M.L. Dalmônico<sup>c</sup>, J. Werckmann<sup>c</sup>, M. Farina<sup>d</sup>, E.A. dos Santos<sup>a,\*</sup>

- a Department of Materials Science and Engineering, Federal University of Sergipe, São Cristóvão, 49100-000, Sergipe, Brazil
- b Department of Mechanical and Industrial Engineering and Department of Bioengineering, University of Illinois at Chicago, Chicago, IL, 60607, United States
- <sup>c</sup> Brazilian Center for Research in Physics, Rio de Janeiro, 22290-180, Rio de Janeiro, Brazil
- <sup>d</sup> Institute of Biomedical Sciences, Federal University of Rio de Janeiro, Rio de Janeiro, 21941-902, Brazil

#### ARTICLE INFO

#### Keywords: Strontium hydroxyapatite Sodium chloride Calcium hydroxyapatite Precipitation Counterions

#### ABSTRACT

The ions found in biological environment during biomineralization as well as the counterions present in syntheses, *i.e.*, the reagents employed, play an important role in the precipitation and stabilization of apatites. In this work, precipitation of strontium-containing hydroxyapatites at different concentrations (0, 20, 40, 60, 80 and  $100\% \, \mathrm{Sr}^{2+}$ ) was performed in the presence of two counterions typically present in biological environments:  $\mathrm{Na}^+$  and  $\mathrm{Cl}^-$ . It was demonstrated that the presence of  $\mathrm{Na}^+/\mathrm{Cl}^-$  in the synthesis environment led to the precipitation of a biphasic hydroxyapatite (HAp) system formed by two non-miscible phases: Ca-rich HAp and Srrich HAp. The biphasic system was observed for intermediate  $\mathrm{Sr}^{2+}$  concentrations (20, 40 and 60%) and exhibited greater lattice microstrain compared with the single-phase systems of Ca HAp (0%) and Sr HAp (100%). Although  $\mathrm{Na}^+/\mathrm{Cl}^-$  were inserted into both Ca- and Sr-rich HAp phases,  $\mathrm{Cl}^-$  ions were preferentially accommodated into the enlarged Sr-rich HAp structure. The presence of  $\mathrm{Cl}^-$  ions in the Sr-rich HAp phase decreased microstrain compared to the Ca-rich phase. After calcination, the biphasic system was transformed into a completely miscible  $\mathrm{Ca/Sr}$  HAp phase without the formation of other phosphates or oxides.

## 1. Introduction

There is abundant evidence that the lattice distortions induced by the replacement of a hydroxyapatite group with a foreign ion can be minimized when multiple ions with different sizes and charges are simultaneously accommodated in the crystal lattice. Aina et al. [1] showed that hydroxyapatites containing Mg $^{2+}$  partially transformed in  $\beta$ -tricalcium phosphate ( $\beta$ -TCP) after heat treatment. However, when Mg $^{2+}$  was inserted into the hydroxyapatite structure simultaneously with Sr $^{2+}$  ions, the phase transformation was significantly decreased. In addition, Kumar et al. [2] found that the simultaneous insertion of Zn $^{2+}$  and CO $_3$  $^{2-}$  into hydroxyapatite decreased the formation of  $\beta$ -TCP and  $\alpha$ -TCP phases after calcination at 1300 °C compared with a pure or Zn $^{2+}$ -doped hydroxyapatite sample.

Kannan et al. [3] studied the cosubstitution of  $\mathrm{Na}^+$  and  $\mathrm{Mg}^{2^+}$  ions in a hydroxyapatite and verified the presence of tricalcium phosphates after calcination above 800 °C. However, it was observed that this simultaneous substitution inhibited the appearance of secondary phases, especially at high temperatures; thus, the simultaneous insertion

stabilized the hydroxyapatite phase. Mostafa et al. [4] also examined cosubstitution of Na $^+$ , SiO<sub>4</sub> $^{4-}$  and CO<sub>3</sub> $^{2-}$  in hydroxyapatite synthesized without atmosphere control (favoring the free insertion of CO<sub>3</sub> $^{2-}$  into the structure). For the SiO<sub>4</sub> $^{4-}$ -containing samples, calcination at 900 °C increased crystallinity but did not induce phase transformation; at 1100 °C, the sample with the highest amount of SiO<sub>4</sub> $^{4-}$  transformed into Ca<sub>5</sub>(PO<sub>4</sub>)<sub>2</sub>SiO<sub>4</sub>. However, the samples containing only Na $^{2+}$  and CO<sub>3</sub> $^{2-}$  showed good thermal stability, which was attributed to the simultaneous insertion of Na $^{2+}$  at the Ca $^{2+}$  sites and CO<sub>3</sub> $^{2-}$  at the PO<sub>4</sub> $^{3-}$ 

In general, authors have explained apatite stabilization by focusing on its behavior after thermal treatment at high temperature, whereas the mechanism of precipitation and stabilization of as-synthesized apatite crystals obtained under conditions of high ionic complexity in aqueous media are not well investigated. Nonetheless, apatite formation in biological environments occurs in the presence of several ions, each has with specific role in apatite precipitation and stabilization, and the properties of different apatite-based deposits in the body (bone, enamel or dentine) are fine-tuned by the presence of these different ions

E-mail address: euler@ufs.br (E.A. dos Santos).

<sup>\*</sup> Corresponding author.

in the apatite lattice [5-7].

 $\mathrm{Sr}^{2+}$  is a trace element in bone mineral; it acts as an inhibitor of osteoclast-resorbing activity and, at the same time, as a stimulator of bone formation by increasing the levels of alkaline phosphatase, type-I collagen and osteocalcin produced by osteoblasts [8,9], justifying its potential use in osteoporosis treatments. For this reason, insertion of  $\mathrm{Sr}^{2+}$  into apatite structures has been receiving particular attention [8,10–13].  $\mathrm{Sr}^{2+}$  ions are able to replace up to 12% of  $\mathrm{Ca}^{2+}$  ions in bone mineral [13], and its stabilization into the apatite lattice appears completely affected by the ionic environment during crystal formation.

For example, Querido et al. [12] observed that the substitution of Ca<sup>2+</sup> for Sr<sup>2+</sup> in a bone-like apatite that was synthesized by osteoblasts in the presence of strontium ranelate occurred simultaneously with the free accommodation of  ${\rm CO_3}^{2-}$  ions into the lattice. Moreira et al. [14] have shown that Sr2+ ion insertion into an apatite lattice along with Mn<sup>2+</sup> and Mg<sup>2+</sup> facilitated the accommodation of the Mn<sup>2+</sup> and Mg<sup>2+</sup> ions, which are known to be difficult to accommodate in apatitic lattices when individually inserted. Recently, Silva et al. [15] observed that two abundant ions in blood plasma (Na<sup>+</sup> and Cl<sup>-</sup>) affected the thermal properties of the Sr-containing hydroxyapatite system. However, the precipitation process itself and the role of these ions in stabilizing the crystals during precipitation were not explained. Therefore, the objective of the present work was to address two important questions: a) how do Na+/Cl- counterions act on the precipitation mechanism of Sr-containing hydroxyapatite crystals in an aqueous medium, and b) how do the initial characteristics of the precipitates affect the thermal stability of the phases?

## 2. Materials and methods

## 2.1. Synthesis of calcium/strontium apatites

To evaluate the effect of counterions present during syntheses on the precipitation of Sr-containing calcium apatites, the procedure described by Silva et al. [15] was employed in this work. In addition to the  $\rm Ca^{2+}$ ,  $\rm PO_4^{3-}$  and  $\rm OH^-$  ions in the synthesis environment,  $\rm Cl^-$  and  $\rm Na^+$  were present as counterions. Hydroxyapatite was prepared by the wet precipitation method under an acid-base reaction between phosphoric acid and calcium chloride. A phosphoric acid solution (0.334 mol  $\rm L^{-1})$  was dropped into a calcium chloride solution (0.220 mol  $\rm L^{-1})$  and kept under stirring at 60 °C without atmospheric control; the pH was maintained at 10.0 by adding sodium hydroxide solution (0.1 mol  $\rm L^{-1})$  during the synthesis. The precipitate was aged for 24 h at 60 °C under stirring. The suspension was filtered, washed with distilled water, and air-dried at 100 °C for 24 h. The dried precipitate was then ground and sieved.

The same procedure was employed for syntheses of the Sr-containing hydroxyapatites. In this case, calcium chloride was gradually replaced with strontium chloride at increasing concentrations (20, 40, 60, 80 and 100 mol %). All reagents were at least 98% pure and purchased from Sigma-Aldrich.

To evaluate the thermal stability of the precipitates, some samples were calcined at  $1000\,^{\circ}\text{C/2}\,\text{h}$  under air at a heating rate of approximately  $3.0\,^{\circ}\text{C/min}$ .

# 2.2. Characterization

## 2.2.1. Elemental composition

The concentration of the elements in the samples was obtained by wavelength-dispersive X-ray fluorescence spectroscopy (WDXRF) using a Bruker S8-Tiger  $4\,\mathrm{kW}$  spectrometer equipped with LiF 200, PET, XS-5 and XS-C crystals. The apatite powders were directly analyzed under a He atmosphere. For quantification, a calibration curve was established using a standard hydroxyapatite (Ca/P = 1.67) powder mixed in 6 different proportions with standard strontium nitrate and sodium chloride powders covering the concentration range of interest for each

element. The powder mixtures were homogenously ground in a ball mill apparatus for 30 min at 350 rpm, and a curve was constructed by analyzing each mixture in powder form under a He atmosphere. Application Wizard software (Bruker) was used to set the X-ray lines and intensity limits for each element and to calculate all statistical parameters. All reagents were of high purity ( $\geq$ 99.5%) and purchased from Sigma-Aldrich.

## 2.2.2. Crystalline structure

The crystalline structure of the samples was assessed by X-ray diffraction (XRD) using a SHIMADZU powder diffractometer. The diffraction patterns were obtained with CuK $\alpha$  (Ni filter) radiation from  $2\theta=10^\circ$  to  $60^\circ$  with a step size of  $0.02^\circ$  and an accumulation time of 2 s/step. The patterns were analyzed using the Rietveld structure refinement method [16,17] and a convolution-based approach for the profile fitting as implemented in HighScore Plus software.

Refinement was conducted from previously known standard structures obtained from Inorganic Crystal Structure Database (ICSD). The structures used included pure calcium apatite  $Ca_{10}(PO_4)_6(OH)_2$  (ICSD  $n^\circ$  151414), pure CaO (ICSD  $n^\circ$  52783), pure strontium apatite  $Sr_{10}(PO_4)_6(OH)_2$  (ICSD  $n^\circ$  2855), and Ca/Sr-containing apatites at different concentrations:  $Ca_8Sr_2(PO_4)_6(OH)_2$  (ICSD  $n^\circ$  86856),  $Ca_6Sr_4(PO_4)_6(OH)_2$  (ICSD  $n^\circ$  86856),  $Ca_6Sr_4(PO_4)_6(OH)_2$  (ICSD  $n^\circ$  155981) and  $Ca_4Sr_6(PO_4)_6(OH)_2$  (ICSD  $n^\circ$  86857). Additional elements, such as Na and Cl, were inserted in the structure files in accordance with WDXRD analyses, respecting the coordinates observed for the host sites in the standard structures. To be consistent with the calcium apatite models, hydrogen was included in the strontium apatite models assuming the position previously established in the calcium apatite standard (ICSD  $n^\circ$  151414). However, to avoid introducing artifacts or unphysical results due to its low scattering, hydrogen coordinates were not refined.

The refined parameters included the following: background (polynomial function with up to 3 coefficients), scale factor, specimen displacement, unit cell parameters (*a* and *c*), peak profile (Caglioti parameters, asymmetry and peak shape), orientation (March-Dollase function), atomic coordinates, and site occupation. Atomic coordinates and occupancies were refined from the heaviest to the lightest atoms.

Occupation by the elements Ca, Sr, P, Na and Cl in the apatite sites was adjusted according to the values measured by WDXRF for each sample. It was assumed that a) Ca [1] and Ca [2] sites could be shared only by the cations  ${\rm Sr}^{2+}$  and  ${\rm Na}^+$ , both under equimolar concentration for each site, and b) Cl-anions could only occupy the hydroxyl positions O [4]H. Occupation of the Ca [1] and Ca [2] sites by  ${\rm Sr}^{2+}$  in the Ca-rich apatite phase and Sr [1] and Sr [2] sites by  ${\rm Ca}^{2+}$  in the Sr-rich apatite phase was calculated from the refinement, and the result is expressed as the  ${\rm Sr}/({\rm Sr} + {\rm Ca})$  ratio.

The crystallite size and lattice strain were estimated from Rietveld refinement considering the changes in the Cagliotti parameters (U and V) between a standard instrument profile and the sample.

## 2.2.3. Fourier transform infrared spectroscopy

The samples were analyzed by FTIR in attenuated total reflectance (ATR) mode using a Perkin-Elmer (Spectrum BX) spectrometer. Analyses were conducted from 4000 to  $400~\rm cm^{-1}$  (step size of  $4~\rm cm^{-1}$ ) to examine the behavior of  $\rm HPO_4^{\ 2-}$ ,  $\rm PO_4^{\ 3-}$ ,  $\rm CO_3^{\ 2-}$  and  $\rm OH^-$  groups. The absorption band positions were based on the previous work of Eichert et al. [18].

# 2.2.4. Morphology and composition of the crystals

The as-synthesized crystals obtained using 40%  $\rm Sr^{2+}$  were observed by scanning transmission electron microscopy (STEM). The analyses were conducted using a JEOL JEM-2100F electron microscope (Brazilian Center for Research in Physics - Brazil) and an aberration-corrected JEOL JEM-ARM200CF electron microscope (University of Illinois at Chicago - USA), both equipped with a field emission gun (FEG) and operated at 200 kV. The elemental composition in different

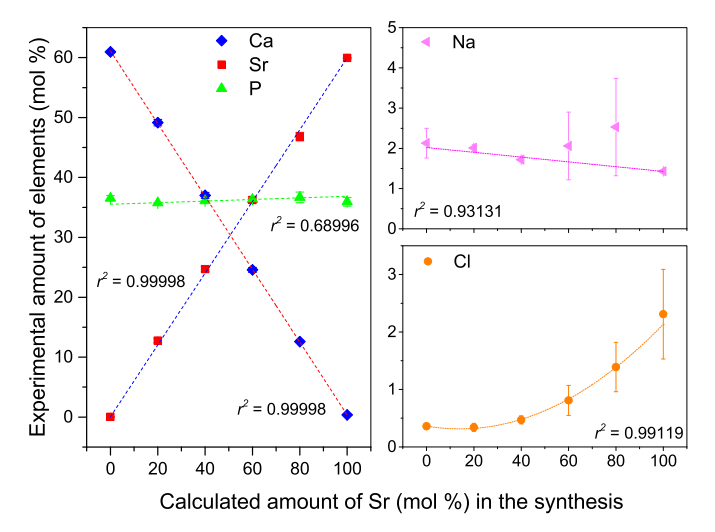


**Fig. 1.** Elemental composition of the apatites prepared in the presence of Na $^+$ /Cl $^-$  with increasing concentrations of Sr $^2$  $^+$ . Na $^+$  and Cl $^-$  were observed in the apatites; they are shown as separate graphics for better visualization. R-square from curve regressions is presented in the graphics.

regions of the crystal agglomerates was obtained by energy dispersive X-ray spectroscopy (EDS).

#### 3. Results and discussion

## 3.1. Elemental and phase composition

The WDXRF analyses allowed for the generation of a profile presenting the evolution of elemental composition of each sample as a function of the calculated amount of Sr for each synthesis (Fig. 1). Ca, P and Sr were identified and quantified in all samples. The amount of Sr increased with the decrease in Ca, which suggested a linear replacement of Ca with Sr. The amount of P increased slightly, but the average cation/P ratio remained constant at approximately 1.68  $\pm$  0.04. The elements Cl and Na were also observed in the composition, indicating their insertion into the precipitate. Although the amount of Na was almost invariable, the amount of Cl increased in the samples with that of Sr.

The sample prepared in the absence of  $Sr^{2+}$ , *i.e.*, Sr/(Sr+Ca)=0, presented a single phase associated with a calcium hydroxyapatite structure, which was termed Ca HAp (Fig. 2). At the same time, the sample prepared in the presence of  $100\% Sr^{2+}$ , *i.e.*, Sr/(Sr+Ca)=1, was formed by a strontium hydroxyapatite single phase, which was termed Sr HAp (refined patterns as supplementary material in Figs. S1–S6). For the intermediate concentrations of  $Sr^{2+}$  (20, 40, 60 and 80%), a gradual displacement of the main diffraction peaks to lower 20 values was observed. This reduction is important evidence of the effective exchange of  $Ca^{2+}$  by  $Sr^{2+}$  ions. With a larger ionic radius than  $Ca^{2+}$  (1.00 Å),  $Sr^{2+}$  (1.18 Å) ions [11,19–21] induce enlargement of interplanar distances (*d*-spacing) when occupying calcium sites in hydroxyapatite structures.

When 20% Sr<sup>2+</sup> or more were used in the synthesis reaction, a Srrich hydroxyapatite (Sr-rich HAp) was obtained. Notably, the main diffraction peaks were split in two, suggesting the precipitation of two distinct populations of crystals with distinct *d*-spacing (Fig. 2). Several factors can lead to diffraction peak displacement. In addition to instrumental errors, peak displacements are related to the modification of *d*-spacings in crystalline materials, and causes of *d*-spacing changes might be the presence of residual stress or of point defects (*e.g.*, substitutional, interstitial elements, vacancies) [22]. Without the presence of stress and defects, preferential orientation (texture) or changes in crystallite size promote peak intensity changes (peak sharpening or

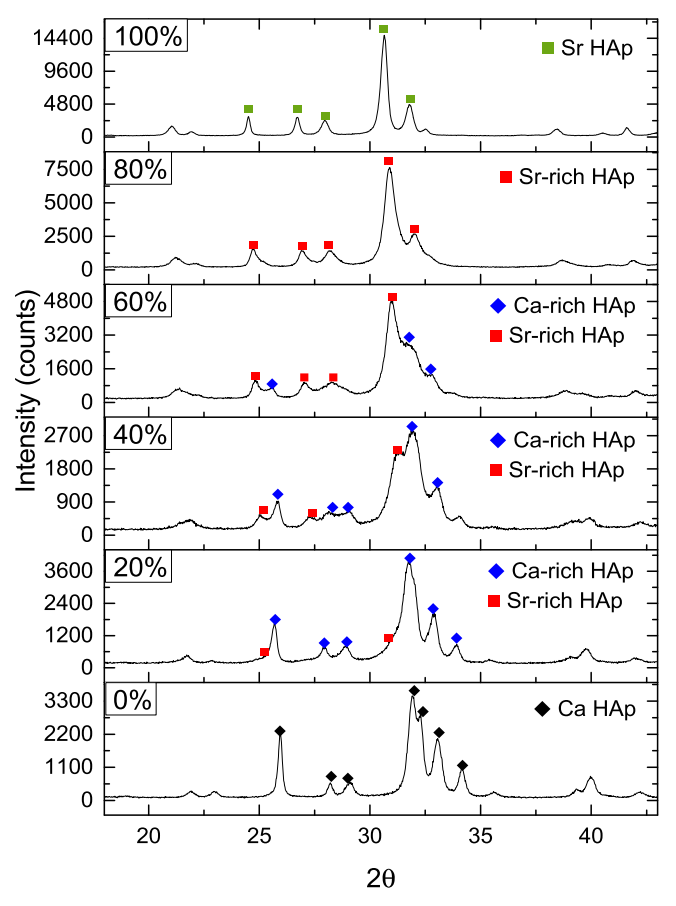


**Fig. 2.** X-ray diffraction pattern of the apatites precipitated in the presence of  $\mathrm{Na}^+/\mathrm{Cl}^-$  with increasing concentrations of  $\mathrm{Sr}^{2+}$ . Note the splitting of several peaks for concentrations from 20% to 60% of  $\mathrm{Sr}^{2+}$ , indicating the formation of a biphasic system (Ca- and Sr-rich HAp). Refined patterns are shown as supplementary data in Figs. S1–S6.

broadening effects) but without modifying the peak positions. All these combined effects are properly considered in the Rietveld method [16,17]. The structural models obtained by Rietveld in our work demonstrated that the main cause of peak displacement was the presence of two distinct apatite phases with different Sr concentrations, both belonging to a hexagonal lattice family with space group P6<sub>3</sub>/m. Two non-miscible apatite phases coexisted in these samples: a Ca-rich HAp and a Sr-rich HAp. The presence of these two phases is most evident when observing syntheses at 40%  $\mathrm{Sr}^{2+}$ , as shown in detail in Fig. 3. The profiles were simulated by assuming the simultaneous presence of these two distinct phases, enabling calculation of the amount of each apatite phase (wt. %) for the entire range of Sr<sup>2+</sup> concentrations obtained via WDXRF (Fig. 4). As expected, gradual insertion of Sr2+ induced an increase in the Sr-rich HAp phase and a decrease in the Ca-rich HAp phase. The low value of  $r^2$  obtained from the linear regression indicated that the precipitation of the two phases is not linear with the concentration of Sr<sup>2+</sup> in the syntheses but rather exponential. When 80% Sr<sup>2+</sup> or more was used, only the Sr-rich HAp phase was observed.

Therefore, the presence of  $\mathrm{Na}^+/\mathrm{Cl}^-$  in the synthesis environment appears to impose restrictions on miscibility, generating different limits of solubility for the ions involved in this process and, consequently, forming a biphasic system. These findings raise the following question: how can a multiphasic system be created as a function of the counterions used?

# 3.2. Occupation of sites in the biphasic system

To better understand the nature of these two crystal populations

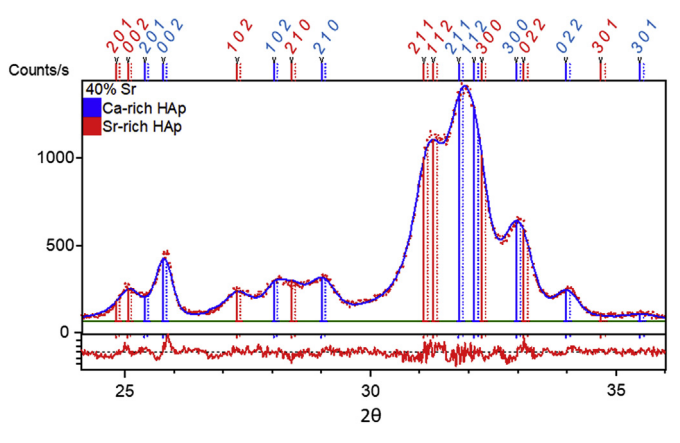


**Fig. 3.** X-ray diffraction details in the region of the main apatite diffraction peaks obtained from samples precipitated in the presence of  $\mathrm{Na}^+/\mathrm{Cl}^-$  under a  $\mathrm{Sr}^{2^+}/(\mathrm{Sr}^{2^+}+\mathrm{Ca}^{2^+})$  ratio of 0.4 (40%  $\mathrm{Sr}^{2^+}$ ). Two different phases were identified: a Ca-rich HAp phase and a Sr-rich HAp phase. The residue (difference) generated from the refinement is shown at the bottom of the graphic. The main diffraction peaks are indexed with the corresponding Miller index for each identified phase on the top of the graphic. A completely refined pattern can be found in the supplementary data (Fig. S3).

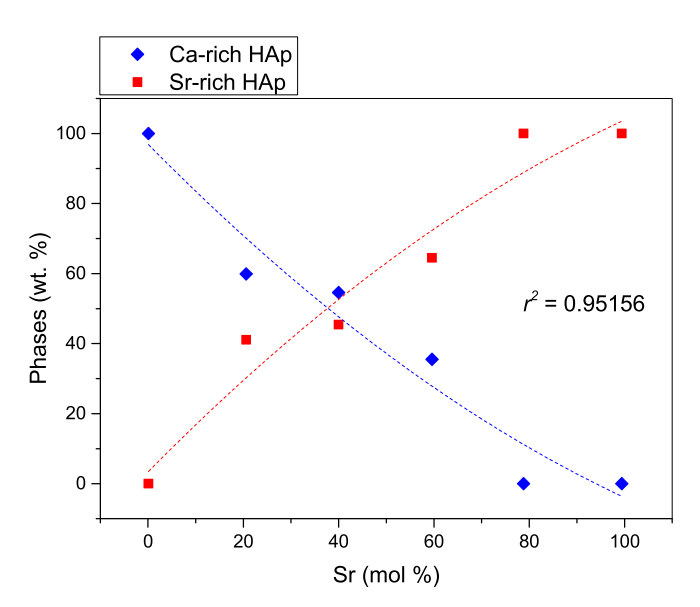
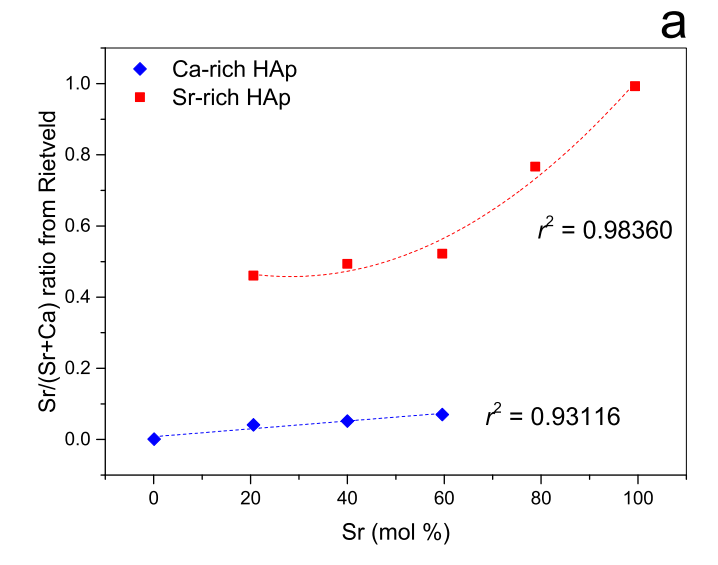


Fig. 4. Evolution of the amount of non-miscible hydroxyapatite phases (Ca- and Sr-rich HAp) coexisting in the precipitate synthesized in the presence of  $\mathrm{Na}^+/\mathrm{Cl}^-$ . The R-square value from curve regression is presented in the graphic.

precipitated in the presence of Na $^+$ /Cl $^-$ , the occupation factors for the Wyckoff positions 4f (Ca [1] and Sr [1] sites) and 4 h (Ca [2] and Sr [2] sites) in the apatite structure were refined, and the initial condition regarding the proportions of the elements was measured by WDXRD. After refining, the relative occupancy values obtained for Sr $^{2+}$ , i.e., Sr/(Sr + Ca) ratios, were used to construct a general occupation profile for each distinct phase as a function of the Sr $^{2+}$  content used in the syntheses (Fig. 5a). From these values, it was possible to observe that the so-called Ca-rich HAp phase contained up to 7% Sr $^{2+}$  atoms distributed between the Ca [1] and Ca [2] sites. At the same time, when 20% Sr $^{2+}$  was available in the synthesis, the so-called Sr-rich HAp phase contained up to 54% Ca $^{2+}$  atoms distributed between the Sr [1] and Sr [2] sites.

The main research to date showing the precipitation of a wide range Sr-containing hydroxyapatites did not report the presence of multiphasic systems in as-precipitated samples [10,15,23,24]. However, in all these works, the syntheses were conducted in the presence of



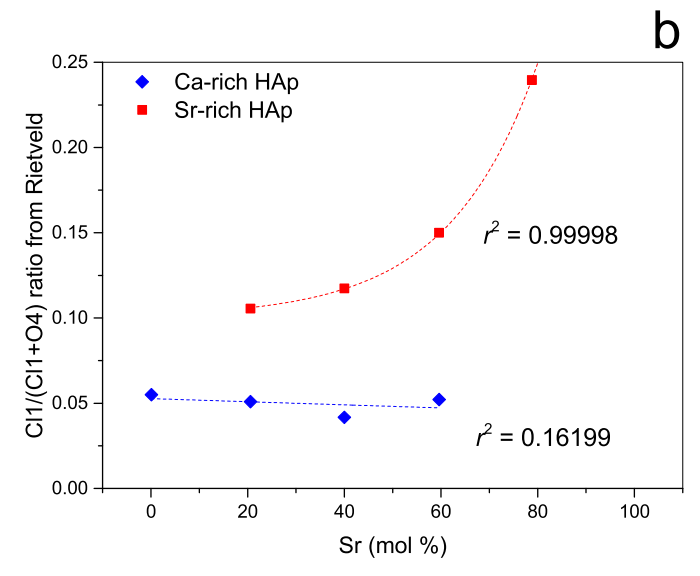


Fig. 5. Relative quantity of  $Sr^{2+}$  (a) and  $Cl^{-}$  (b) present in each non-miscible precipitated phase (Ca- and Sr-rich HAp) at increasing  $Sr^{2+}$  concentrations. The values were calculated from Rietveld refinement using Ca [1], Ca [2], Sr [1], Sr [2], O [4] and Cl [1] occupancy levels. R-squares obtained from curve regressions are presented in the graphic.

counterions known to be difficult to insert into the apatite lattice, notably NH<sub>4</sub> +/NO<sub>3</sub>. Therefore, it seems reasonable to associate the coexistence of the two populations of crystals found in our work with the presence of Na<sup>+</sup>/Cl<sup>-</sup>, especially because WDXRD analyses identified these ions in the precipitates. For this reason, these two elements were also included in the structure files used in the simulations. Na<sup>+</sup> ions were assumed to replace Ca<sup>2+</sup> in both the Ca [1] - Ca [2] and Sr [1] - Sr [2] positions of the Ca-rich and Sr-rich HAp phases, and Cl<sup>-</sup> ions were expected to replace the hydroxyl groups in the Wyckoff position 4e (O [4]H) for both phases. The low convergence of the statistical indices obtained for these initial conditions indicated that insertion of similar amounts of Cl<sup>-</sup> ions at the hydroxyl sites for both Ca- and Sr-rich HAp phases was extremely unfavorable. Indeed, the statistical indices for the refinement were improved only after simulating the occupancy of the OH groups with different proportions of Cl ions, indicating that each hydroxyapatite phase must have different abilities to capture Cl ions from the aqueous medium during precipitation. After calculating the

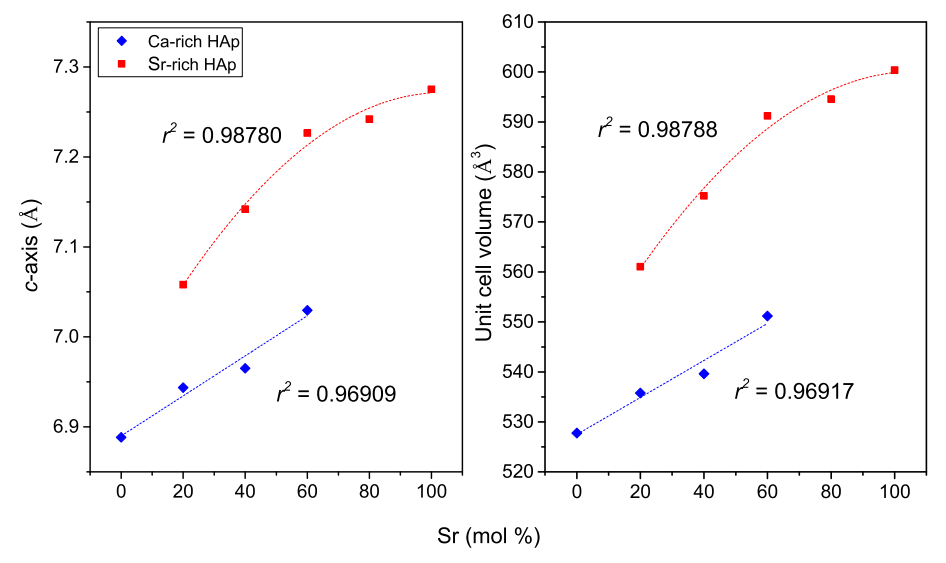
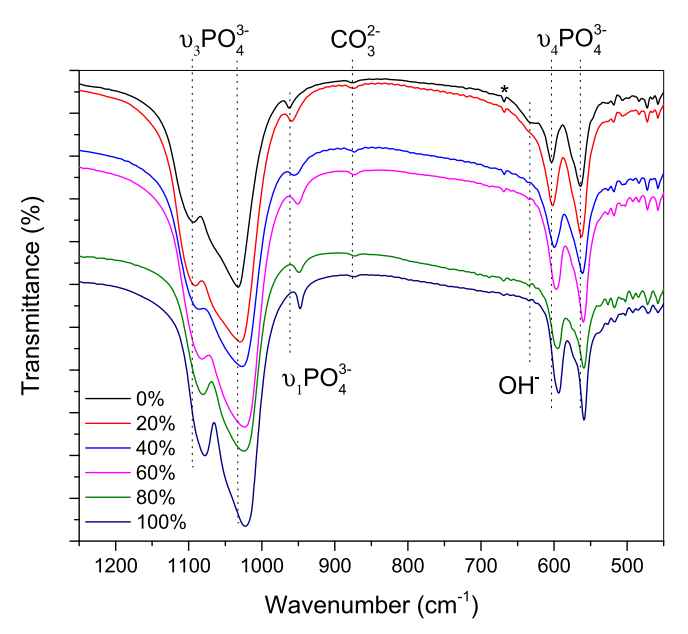


Fig. 6. Unit cell volumes and c-axes calculated from Rietveld refinement for two non-miscible precipitated phases (Ca- and Sr-rich HAp) at increasing  $Sr^{2+}$  concentrations. R-squares obtained from curve regressions are presented in the graphic.

relative level of Cl<sup>-</sup> for each phase, *i.e.*, the Cl [1]/(Cl [1]+O [4]) occupancy ratio, it was concluded that the Ca-rich HAp supported fewer Cl<sup>-</sup> ions in its structure than did the so-called Sr-rich HAp phase, as shown in Fig. 5b. The low value of  $r^2$  obtained from the Ca-rich HAp curve indicates that insertion of the Cl<sup>-</sup> ion in this phase was not affected by the concentration of Sr<sup>2+</sup> in the syntheses. Conversely, the level of Cl<sup>-</sup> ions in the Sr-rich HAp phase grew exponentially with increasing Sr<sup>2+</sup> concentration. For Ca-rich HAp, up to 5.2% of the hydroxyl groups were replaced with Cl<sup>-</sup> ions, which was a low value compared to the 53% observed for the Sr-rich HAp phase. This is very interesting because uptake of Cl<sup>-</sup> ions by biological calcium apatites is very low (up to 0.25 wt%) [25] compared with the high level of Cl<sup>-</sup> ions in the blood [26]. Therefore, the increase in Sr<sup>2+</sup> in the Sr-rich HAp induced a stronger uptake of Cl<sup>-</sup> ions from the aqueous medium, as indicated by WDXRD results (Fig. 1).

The lattice expansion promoted by the insertion of  $\mathrm{Sr}^{2+}$  ions into the apatite lattice induced a marked increase in the c-axis and unit cell volume of both non-miscible HAp phases (Fig. 6). The parameters measured for the Ca-rich HAp phase exhibited linear growth, with exponential growth observed for the Sr-rich phase. This behavior suggests that the increase in  $\mathrm{Sr}^{2+}$  ions in the lattice was not the only factor contributing to the increase in volume of the Sr-rich phase. As suggested by the Rietveld refinement, the Sr-rich HAp phase captured more  $\mathrm{Cl}^-$  during growth than did the Ca-rich phase. Because  $\mathrm{Cl}^-$  ions (1.81 Å) are larger than  $\mathrm{OH}^-$  groups (1.31 Å) [15,19], the replacement of  $\mathrm{OH}^-$  groups for  $\mathrm{Cl}^-$  ions contributed to increasing the parameters of the Sr-rich HAp phase.

The PO<sub>4</sub><sup>3-</sup> and OH<sup>-</sup> groups of apatites were observed on the precipitates by FTIR (Fig. 7). The  $\nu_{4}$ -as symetric bending mode of the O-P-O groups of PO<sub>4</sub><sup>3-</sup> appeared as three absorption bands at 565, 571, and  $602 \, \mathrm{cm}^{-1}$  [27]; the modes  $v_1$  and  $v_3$  of  $PO_4{}^{3-}$  were observed between 960 and 1150 cm<sup>-1</sup> [21,22]. A remarkable displacement of the peaks to regions of lower frequency was observed for increasing amounts of Sr2+, and this red shift was expected because Sr2+ is larger than Ca<sup>2+</sup>. At 632 cm<sup>-1</sup>, a band related to the O-H translational mode (libration) of the hydroxyl groups ( $\nu_I OH^-$ ) [28] was observed. This band appeared as a shoulder at  $0\%\ Sr^{2+}$  and gradually disappeared with increasing Sr<sup>2+</sup> concentration. As suggested by the Cl [1]/(Cl [1] +O [4]) occupancy ratio estimated by Rietveld, the replacement of OH groups for Cl can explain this behavior. Additionally, a band at  $875 \,\mathrm{cm}^{-1}$  associated with the  $\nu_2$ -out-of-plane bending vibration of O-C-O groups from  ${\rm CO_3}^2$  [28,29] was observed for all precipitates, confirming the insertion of carbonate in the apatite structure. In



**Fig. 7.** FTIR spectra obtained from as-synthesized precipitates for increasing  ${\rm Sr}^{2+}$  concentrations. Zoomed regions show the main absorption modes from  ${\rm PO_4}^{3-}$ ,  ${\rm OH}^-$ ,  ${\rm CO_3}^{2-}$  groups. \*Carbon dioxide absorption from the environment (667 cm $^{-1}$ ).

general, insertion of monovalent cations into HAp, such as  $\mathrm{Na}^+$ , is followed by insertion of  $\mathrm{CO_3}^{2-}$ , especially at  $\mathrm{PO_4}^{3-}$  sites [30,31]. This simultaneous insertion also generates  $\mathrm{OH}^-$  vacancies and warrants the charge imbalance required to form a neutral crystal. Therefore, the model proposed by Rietveld is in accordance with our results from WDXRF and FTIR, even though the large quantity of vibrational modes in these regions broadened the absorption bands, making it difficult to differentiate signals coming from either Ca- or Sr-rich HAp phases.

STEM and EDS were utilized to observe the distribution of Ca and Sr along the crystals (Fig. 8). Clearly, the intensity of the X-ray signals emitted from Ca ( $Ca_{K\alpha 1}$ ) and Sr ( $Sr_{K\alpha 1}$ ) atoms were remarkably different at different regions of the crystal agglomerates. These differences are directly related to concentration changes, confirming the presence of distinct Ca- and Sr-rich regions on the crystal agglomerates, as suggested by X-ray diffraction. Calculation of the relative molar amount of Sr, *i.e.*, the Sr/(Sr + Ca) ratio from EDS, once more confirmed the

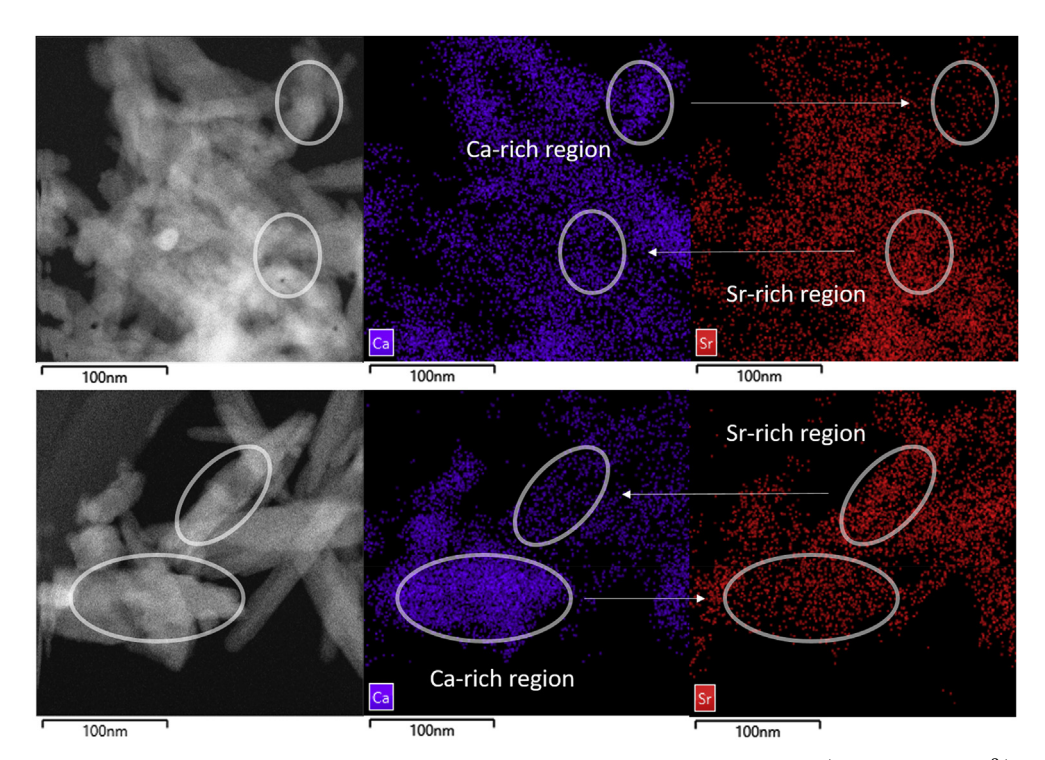
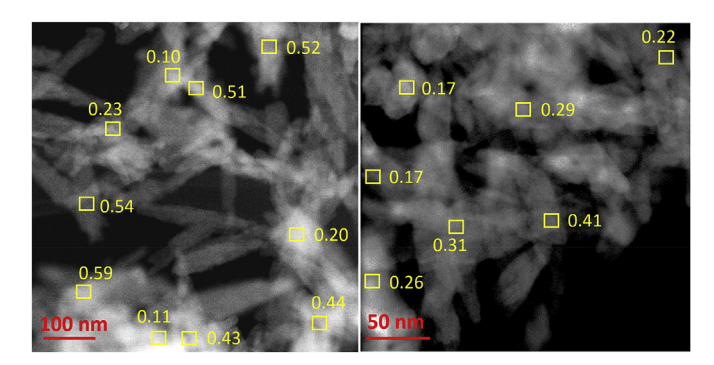


Fig. 8. STEM image and EDS elemental maps of Ca and Sr obtained from crystals precipitated in the presence of Na $^+$ /Cl $^-$  at 40% of Sr $^{2+}$ . Intensity differences of Ca<sub>K $\alpha$ 1</sub> and Sr <sub>K $\alpha$ 1</sub> X-ray emission lines at distinct regions of the apatite crystals demonstrate changes in the Sr/(Sr + Ca) ratio, as indicated in Ca- and Sr-rich regions.



**Fig. 9.** STEM images and EDS analyses obtained from crystals precipitated in the presence of Na $^+$ /Cl $^-$  at 40% Sr $^{2+}$ . The values depicted in the different regions of the images express the Sr/(Sr $^+$  Ca) ratio calculated from EDS spectra for Ca<sub>K $\alpha$ 1</sub> and Sr $^+$ <sub>K $\alpha$ 1</sub> X-ray emission lines.

heterogeneous concentration of Sr along the different regions of the crystal agglomerates (Fig. 9). As shown previously (Fig. 5a), at a level of 40% Sr<sup>2+</sup>, the Ca-rich HAp phase accommodated approximately 6% Sr2+ in its structure, but the Sr-rich HAp phase accommodated approximately 50% Sr2+. The lower Sr2+ concentration in the crystal agglomerates found by EDS was 10%, which is close to the value expected for the Ca-rich HAp phase. The intermediate values found between 10% and 50% reflected the polycrystalline nature of the agglomerates and the superposition of different crystals belonging to both Ca- and Sr-rich phases. The average of the Sr/(Sr + Ca) ratio calculated from EDS for the whole image was approximately 38.9%, which is very close to the value determined via WDXRF (40.0%). Thus, the heterogeneity in Sr<sup>2+</sup> concentration observed for the samples precipitated in the presence of Na<sup>+</sup>/Cl<sup>-</sup> is very strong evidence of the presence of the two crystal populations, as previously demonstrated by XRD and Rietveld refinement.

The precipitation kinetics of hydroxyapatite crystals are predominantly driven by a polynucleation process rather than by a growth process [32,33]. The growth is achieved by the agglomeration of calcium phosphate nanoclusters [32,34,35], which tend to nucleate and crystallize. Therefore, the presence of a biphasic system can be supported by the fact that during precipitation, several nanoclusters and nuclei with different proportions of Ca<sup>2+</sup> and Sr<sup>2+</sup> can be simultaneously formed, as driven by saturation of the local environment with the ions present in the solution. Pan et al. [23] detected Ca2+ incorporated into an apatite that spontaneously precipitated onto solid particles of strontium hydroxyapatite in simulated body fluid (SBF). However, no Sr2+ was detected in the apatite precipitated onto solid particles of a calcium hydroxyapatite, even when Sr<sup>2+</sup> ions were present in the SBF solution. This result indicated that the accommodation of Ca<sup>2+</sup> into a Sr-rich apatite lattice is always energetically more favorable than the accommodation of Sr<sup>2+</sup> into a Ca-rich apatite lattice. As the solubility of Sr HAp is greater than that of Ca HAp [23], the nucleation of the former is less favorable than that of the latter. In fact, the enthalpy of formation  $\Delta_f H^0$  (298 K) for  $Sr_{10}(PO_4)_6(OH)_2$  $(-13371 \text{ kJ mol}^{-1})$  is slightly larger than for  $Ca_{10}(PO_4)_6(OH)_2$  $(-13305\,\mathrm{kJ\,mol^{-1}})$  and is much larger than for  $\mathrm{Sr_{10}(PO_4)_6Cl_2}$  $(-13233 \,\mathrm{kJ} \,\mathrm{mol}^{-1})$  [36]. Considering that the composition of SBF solutions is very complex and that these solutions contain different ions such as Na+, Cl- and CO32-, one can assume that the saturation condition required to form a Sr-rich HAp containing  $\mathrm{Cl}^-$  ions is more easily achieved than to form a strontium hydroxyapatite free of Cl-. However, the subsequent shortage of Sr<sup>2+</sup> and Cl<sup>-</sup> ions in the crystal growth front can create a new saturation condition that favors the formation of Ca-rich HAp. A similar behavior is observed in solid-state transformation, as either discontinuous precipitation [37] or periodic precipitation can occur under growth-rate oscillations [38,39]. This may explain why it was difficult to observe isolated Ca- and Sr-rich crystals in the agglomerates, which generated a heterogeneous Sr/ (Sr + Ca) ratio distribution.

## 3.3. Biphasic precipitates transformed into monophasic after calcination

After thermal treatment at  $1000\,^{\circ}$ C for 2 h, the precipitates obtained in the presence of Na $^+$ /Cl $^-$ , which were originally composed of a

Ceramics International 46 (2020) 4502–4510

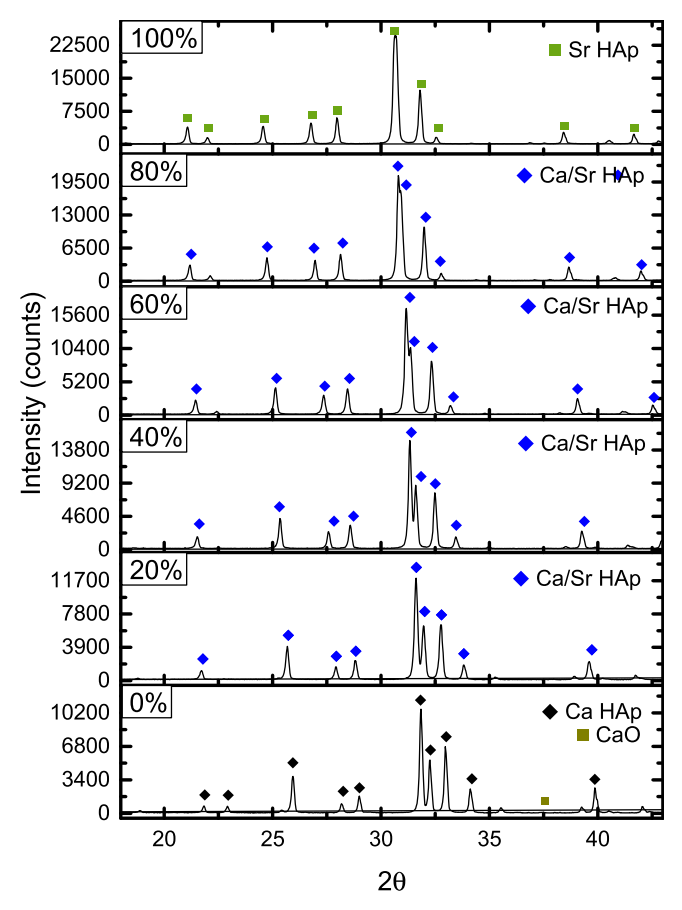


**Fig. 10.** X-ray diffraction pattern of apatites precipitated in the presence of Na $^+$ /Cl $^-$  with increasing concentrations of Sr $^{2+}$  after thermal treatment at  $1000\,^{\circ}$ C/2 h. Note the complete miscibility of Ca $^{2+}$  and Sr $^{2+}$  for concentrations from 20% to 80% of Sr $^{2+}$ . The presence of 0.1 wt % CaO was detected in the sample without Sr $^{2+}$  (0.0% Sr $^{2+}$ ). Refined patterns are shown as supplementary data in Figs. S7–S12.

biphasic population of apatite crystals (Ca-rich HAp and Sr-rich HAp), were transformed into a single phase of Sr-containing hydroxyapatite (Ca/Sr HAp) (Fig. 10). Only a slight transformation occurred for the sample produced in the absence of  $\rm Sr^{2+}$  (0%  $\rm Sr^{2+}$ ), forming approximately 0.1 wt % of CaO. After the insertion of  $\rm Sr^{2+}$ , no transformation was detectable in the samples.

The shortage of cations in apatites is the main cause of phase transformation at high temperature, producing  $\alpha\text{-/}\beta\text{-tricalcium}$  phosphates ( $\alpha\text{-TCP}$  and  $\beta\text{-TCP}$ ). In our case, the cation/P ratio was maintained at approximately 1.68  $\pm$  0.04 for all samples. The absence of  $\alpha\text{-}$  or  $\beta\text{-TCP}$  phases in our samples demonstrated that the apatite stoichiometry, notably the cation/P ratio, was not significantly altered by the presence of the different ions. The insertion of  $\text{CO}_3^{\,2^-}$  and consequent formation of  $\text{Ca}^{2^+}$  and  $\text{OH}^-$  vacancies, along with the insertion of  $\text{Sr}^{2^+}$ ,  $\text{Na}^+$  and  $\text{Cl}^-$ , appeared to create the necessary conditions to avoid important changes in stoichiometry and, consequently, phase transformation.

Therefore, the two populations of crystals (Ca-rich HAp and Sr-rich HAp) combined at high temperature to form a completely miscible Ca/Sr HAp phase without the presence of other phases. In general, multiphasic systems tend to increase barriers to diffusion, which decreases homogenization of the elements and consequently leads to the maintenance of multiphasic systems [20,40]. Such behavior is related to systems in which the different phases belong to different crystal lattice families and have different chemical compositions. In our case, the presence of Na $^+/\text{Cl}^-$  induced the precipitation of a biphasic system composed of two non-miscible hydroxyapatites [41]. Regardless of the

composition, all apatites obtained had a hexagonal lattice structure with space group  $P6_3/m$ . Therefore, barriers to diffusion are not so high, especially if we assume the nanometric nature of the crystals confined in an aqueous environment, as presented in Figs. 8–9. The smaller is the crystallite size, the higher is the surface energy available to promote diffusion at high temperature.

As introduced before, diffraction peak broadening can reflect an association among instrumental settings, crystalline domain sizes and lattice defects induced by microstrains [42]. After removing the instrumental contribution, it is possible to consider that the crystalline domain size (coherence length) is the major contributor to the broadening effect for nanocrystals. In these cases, the Scherrer equation can be applied to estimate the crystallite size. However, Kim et al. [43] demonstrated that the Scherrer equation should not be used when lattice microstrains are also present, especially for coprecipitated systems in which crystals can be doped during their growth. Indeed, doping can produce a large number of structural points and linear defects, generating microstrains that contribute to peak broadening in a similar manner to crystallite size. In these cases, the distinction between crystallite size and lattice microstrains can be better estimated from Rietveld refinement by considering changes in the Cagliotti parameters (U and V). For this reason, both crystallite size and lattice microstrains were calculated in this work based on the Rietveld refinement.

In general, the as-synthesized precipitates formed in the presence of  $\mathrm{Na}^+/\mathrm{Cl}^-$  presented crystallite sizes smaller than 35 nm for both Ca-and Sr-rich HAp phases (Fig. 11). At the same time, the highest lattice microstrains were verified for intermediate  $\mathrm{Sr}^{2+}$  concentrations. A reduction in crystallite size and increase in lattice microstrain directly reflects a decrease in crystallinity caused by the nonperfect ordering of the crystalline arrays [44]; the mere presence of two populations of non-miscible nanocrystals in intermediate concentrations also contributes to higher system disorder.

Nimmy et al. [10] showed that Sr-containing hydroxyapatite crystals experience stronger sonofragmentation at intermediate Sr<sup>2+</sup> concentrations. After calculating the density of dislocations in the crystals as a function of the Sr2+ concentration, they demonstrated that the amount of dislocations was larger for these intermediate concentrations, attributing the higher crystal sonofragmentation to the high amount of these linear defects generated when Ca<sup>2+</sup> or Sr<sup>2+</sup> are present in equimolar quantities. Zeglinski et al. [45] also demonstrated using ab initio and Rietveld refinement that insertion of Sr2+ into a calcium hydroxyapatite lattice is an endothermic process and that the maximum of excess energy is observed for equimolar concentrations. This high energy may be directly associated with greater structural instability. Furthermore, Frasnelli et al. [24] showed that the line broadening (FWHM) of the deconvoluted main components of <sup>31</sup>P and <sup>1</sup>H NMR spectra, i.e., the structural disorder around PO<sub>4</sub><sup>3-</sup> and OH<sup>-</sup> environments in apatites, is more preeminent when Ca<sup>2+</sup> and Sr<sup>2+</sup> are in equimolar concentrations.

According to these findings, intermediate Sr<sup>2+</sup> concentrations tend to introduce a higher level of disorder in the apatites obtained. This is in accordance with our results showing a remarkable increase in lattice microstrains at intermediate concentrations or concentrations close to the solubility limit; notably, this was observed for the Ca-rich HAp, which contained approximately 6% Sr<sup>2+</sup>, and the Sr-rich HAp phase, which accommodated approximately 50% Ca2+ (Fig. 5a). However, it was also possible to observe that the Sr-rich HAp phase experienced a strong reduction in microstrain at increasing Sr<sup>2+</sup> concentrations (Fig. 11). The simultaneous insertion of Cl<sup>-</sup> ions into the Sr-rich HAp phase lattice appeared to favor a lattice relaxation, opposing the higher strains caused by insertion of Sr<sup>2+</sup> in the Ca-rich HAp phase. After calcination, the Ca/Sr HAp phase generated from the transformation of the biphasic system (Fig. 10) presented even more relaxed lattices (lower microstrains) and larger crystallite sizes (Fig. 11). The high temperature favored diffusion and helped to mix both Ca- and Sr-rich phases, creating a completely miscible Ca/Sr HAp. One could assume

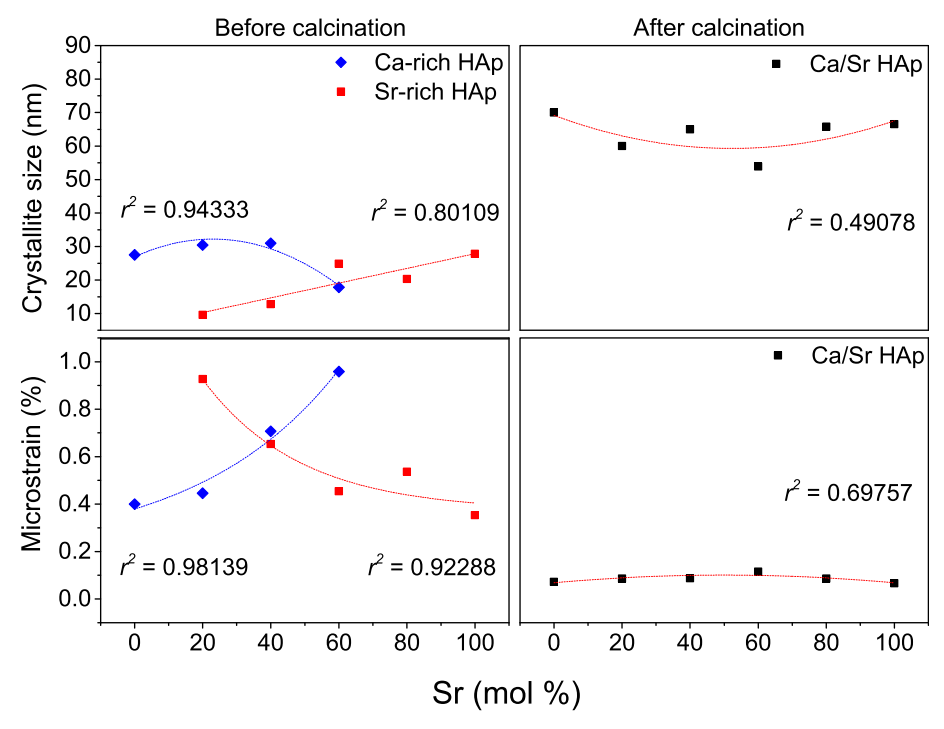


Fig. 11. Crystallite size and lattice microstrains calculated by Rietveld refinement from each apatite phase synthesized in the presence Na<sup>+</sup>/Cl<sup>-</sup> before (left) and after (right) calcination at 1000 °C/2 h. R-squares obtained from curve regressions are presented in the graphic.

that the higher microstrains at intermediate  $\mathrm{Sr}^{2+}$  concentrations and the balance between the microstrains in both phases were the driving force involved in this transformation. Therefore, the insertion of  $\mathrm{Na}^+$  and  $\mathrm{Cl}^-$  ions along with the substitution of  $\mathrm{Ca}^{2+}$  for  $\mathrm{Sr}^{2+}$  into the apatite lattice increased the disorder of the system during crystal growth but favored the formation of a more relaxed lattice after calcination, allowing the formation of a miscible  $\mathrm{Ca/Sr}$  HAp phase.

Overall, our results demonstrate that apatitic systems are greatly affected by the presence of different ions in solution during the precipitation process. Unlike other ceramic systems, hydroxyapatite is able to simultaneously capture and accommodate several ions in its structure. The spontaneous insertion of such ions with different charges and sizes during precipitation can further determine the stability of the phases obtained, being an important means for controlling undesirable phase transformations during processing and, at the same time, warranting conditions to enrich apatite with several ions of biological interest.

# 4. Conclusions

The presence of Na $^+$ /Cl $^-$  in the synthesis environment led to the precipitation of a biphasic hydroxyapatite (HAp) system formed by two non-miscible phases: Ca-rich HAp and Sr-rich HAp. The biphasic system was observed for intermediate Sr $^{2+}$  concentrations (20, 40 and 60%) and exhibited higher lattice microstrains compared with the single-phase systems of Ca HAp (0%) and Sr HAp (100%). Although Na $^+$ /Cl $^-$  were inserted into both Ca- and Sr-rich HAp phases, Cl $^-$  ions were preferentially accommodated into the enlarged Sr-rich HAp structure. The presence of Cl $^-$  ions in the Sr-rich HAp phase decreased microstrains compared to the Ca-rich phase. After calcination, the biphasic system was transformed into a completely miscible Ca/Sr HAp phase without the formation of other phosphates or oxides.

### Data availability

Supplementary material containing the Rietveld refinement data is accessible in the electronic version of the manuscript. Raw data will be

made available on request to the corresponding author.

## **Declaration of competing interest**

The authors declare that they have no known competing financial interests or personal relationships that could have appeared to influence the work reported in this paper.

## Acknowledgments

The authors acknowledge financial support from the Brazilian research agencies FAPITEC/SE, CAPES, and CNPq in the form of the grants PROMOB CAPES/FAPITEC-SE (Nº 88881.157913/2017-01) and PDE/CNPq (N° 205536/2018-2). R. Shahbazian-Yassar, T. Shokuhfar, and S. Narayanan's efforts were funded by National Science Foundation (NSF)-Biomaterials Program (BMAT) under Award N° 1710049. The authors also acknowledge LABNANO at the Brazilian Center for Research in Physics (CBPF) for the use of the JEOL JEM-2100F transmission electron microscope and the University of Illinois at Chicago. JEOL JEM-ARM200CF in the Electron Microscopy Core of UIC's Research Resources Center was also used in this work. The acquisition of this instrument was supported by an MRI-R2 grant from the National Science Foundation (DMR-0959470).

## Appendix A. Supplementary data

Supplementary data to this article can be found online at https://doi.org/10.1016/j.ceramint.2019.10.177.

### References

- [1] V. Aina, G. Lusvardi, B. Annaz, I.R. Gibson, F.E. Imrie, G. Malavasi, L. Menabue, G. Cerrato, G. Martra, Magnesium- and strontium-co-substituted hydroxyapatite: the effects of doped-ions on the structure and chemico-physical properties, J. Mater. Sci. Mater. Med. 23 (2012) 2867–2879, https://doi.org/10.1007/s10856-012-4767-3.
- [2] G.S. Kumar, A. Thamizhavel, Y. Yokogawa, S.N. Kalkura, E.K. Girija, Synthesis, characterization and in vitro studies of zinc and carbonate co-substituted nanohydroxyapatite for biomedical applications, Mater. Chem. Phys. 134 (2012)

- 1127-1135, https://doi.org/10.1016/j.matchemphys.2012.04.005.
- [3] S. Kannan, J.H.G.G. Rocha, J.M.F.F. Ferreira, Synthesis and thermal stability of sodium, magnesium co-substituted hydroxyapatites, J. Mater. Chem. 16 (2006) 286–291, https://doi.org/10.1039/B511867K.
- [4] N.Y. Mostafa, H.M. Hassan, O.H. Abd Elkader, Preparation and characterization of Na+, SiO44-, and CO32-Co-substituted hydroxyapatite, J. Am. Ceram. Soc. 94 (2011) 1584–1590, https://doi.org/10.1111/ji.1551-2916.2010.04282.x.
- [5] B.N. Bachra, H.R.A. Fischer, The effect of some inhibitors on the nucleation and crystal growth of apatite, Calcif. Tissue Res. 3 (1969) 348–357, https://doi.org/10. 1007/BF02058677.
- [6] D.R. Eisenmann, J.A. Yaeger, Alterations in the formation of rat dentine and enamel induced by various ions, Arch. Oral Biol. 14 (1969), https://doi.org/10.1016/0003-9969(69)90075-2 1045–IN13.
- [7] Mann Stephen, Biomineralization: Principles and Concepts in Bioinorganic Materials Chemistry, Oxford University Press, New York, 2001.
- [8] W. Zhang, Y. Shen, H. Pan, K. Lin, X. Liu, B.W. Darvell, W.W. Lu, J. Chang, L. Deng, D. Wang, W. Huang, Effects of strontium in modified biomaterials, Acta Biomater. 7 (2011) 800–808, https://doi.org/10.1016/j.actbio.2010.08.031.
- [9] S. Pors Nielsen, The biological role of strontium, Bone 35 (2004) 583–588, https://doi.org/10.1016/j.bone.2004.04.026.
- [10] N. Edwin, P. Wilson, Investigations on sonofragmentation of hydroxyapatite crystals as a function of strontium incorporation, Ultrason. Sonochem. 50 (2019) 188–199, https://doi.org/10.1016/j.ultsonch.2018.09.018.
- [11] E. Boanini, M. Gazzano, A. Bigi, Ionic substitutions in calcium phosphates synthesized at low temperature, Acta Biomater. 6 (2010) 1882–1894, https://doi.org/10. 1016/j.actbio.2009.12.041.
- [12] W. Querido, A.P.C. Campos, E.H. Martins Ferreira, R.A.S. San Gil, A.M. Rossi, M. Farina, Strontium ranelate changes the composition and crystal structure of the biological bone-like apatite produced in osteoblast cell cultures, Cell Tissue Res. 357 (2014) 793–801, https://doi.org/10.1007/s00441-014-1901-1.
- [13] D. Farlay, G. Boivin, G. Panczer, A. Lalande, P.J. Meunier, Long-term strontium ranelate administration in monkeys preserves characteristics of bone mineral crystals and degree of mineralization of bone, J. Bone Miner. Res. 20 (2005) 1569–1578, https://doi.org/10.1359/JBMR.050405.
- [14] M.P. Moreira, G.D. de Almeida Soares, J. Dentzer, K. Anselme, L.Á. de Sena, A. Kuznetsov, E.A. dos Santos, Synthesis of magnesium- and manganese-doped hydroxyapatite structures assisted by the simultaneous incorporation of strontium, Mater. Sci. Eng. C 61 (2016) 736–743, https://doi.org/10.1016/j.msec.2016.01.
- [15] L.M. da Silva, D. dos Santos Menezes, L.E. Almeida, K. Anselme, J. Dentzer, E.A. dos Santos, The role of the counter-ions present in syntheses on the thermal stabilization of strontium and/or calcium apatites, Mater. Sci. Eng., B 199 (2015) 77–86, https://doi.org/10.1016/j.mseb.2015.05.003
- [16] H.M. Rietveld, Line profiles of neutron powder-diffraction peaks for structure refinement, Acta Crystallogr. 22 (1967) 151–152, https://doi.org/10.1107/ S0365110X67000234.
- [17] R.A. Young, The Rietveld Method, Oxford University Press, New York, 1993.
- [18] D. Eichert, C. Drouet, H. Sfihi, C. Rey, C. Combes, Nanocrystalline Apatite-Based Biomaterials, UK ed., Nova Science Publishers, Inc., New York, 2009.
- [19] J.C. Elliott, Structure and Chemistry of the Apatites and Other Calcium Orthophosphates, ELSEVIER, London, UK, 1994.
- [20] Y.-M. Chiang, D. Birnie, W.D. Kingery, Principles for Ceramic Science and Engineering, John Wiley & Sons, Boston, 1997.
- [21] B. Bracci, P. Torricelli, S. Panzavolta, E. Boanini, R. Giardino, A. Bigi, Effect of Mg2+, Sr2+, and Mn2+ on the chemico-physical and in vitro biological properties of calcium phosphate biomimetic coatings, J. Inorg. Biochem. 103 (2009) 1666–1674, https://doi.org/10.1016/j.jinorgbio.2009.09.009.
- [22] B.D. Cullity, Elements of X-Ray Diffraction, second ed., Addison-Wesley Publishing Company, Michigan, 1978.
- [23] H.B. Pan, Z.Y. Li, W.M. Lam, J.C. Wong, B.W. Darvell, K.D.K. Luk, W.W. Lu, Solubility of strontium-substituted apatite by solid titration, Acta Biomater. 5 (2009) 1678–1685, https://doi.org/10.1016/j.actbio.2008.11.032.
- [24] M. Frasnelli, F. Cristofaro, V.M. Sglavo, S. Dirè, E. Callone, R. Ceccato, G. Bruni, A.I. Cornaglia, L. Visai, Synthesis and characterization of strontium-substituted hydroxyapatite nanoparticles for bone regeneration, Mater. Sci. Eng. C 71 (2017) 653–662, https://doi.org/10.1016/j.msec.2016.10.047.

- [25] R. Zapanta LeGeros, Apatites in biological systems, Prog. Cryst. Growth Charact. 4 (1981) 1–45, https://doi.org/10.1016/0146-3535(81)90046-0.
- [26] P. a a P. Marques, M.C.F. Magalhães, R.N. Correia, Inorganic plasma with physiological CO2/HCO3- buffer, Biomaterials 24 (2003) 1541–1548 doi:S0142961202005392 [pii].
- [27] M. Corno, C. Busco, B. Civalleri, P. Ugliengo, Periodic ab initio study of structural and vibrational features of hexagonal hydroxyapatite Ca10(PO4)6(OH) 2, Phys. Chem. Chem. Phys. 8 (2006) 2464–2472, https://doi.org/10.1039/b602419j.
- [28] M.E. Fleet, Infrared spectra of carbonate apatites: ??2-Region bands, Biomaterials 30 (2009) 1473–1481, https://doi.org/10.1016/j.biomaterials.2008.12.007.
- [29] H. Madupalli, B. Pavan, M.M.J.J. Tecklenburg, Carbonate substitution in the mineral component of bone: discriminating the structural changes, simultaneously imposed by carbonate in A and B sites of apatite, J. Solid State Chem. 255 (2017) 27–35, https://doi.org/10.1016/j.jssc.2017.07.025.
- [30] M.E. Fleet, X. Liu, Coupled substitution of type A and B carbonate in sodiumbearing apatite, Biomaterials 28 (2007) 916–926, https://doi.org/10.1016/j. biomaterials.2006.11.003.
- [31] F.B. Simões, L.M. da Silva, T.O. Fonseca, L.E. Almeida, E.A. dos Santos, Isolated effects of microwave radiation on the solid-liquid interface reactions between hydroxyapatite nanocrystals and silver ions, Ceram. Int. 44 (2018) 16960–16971, https://doi.org/10.1016/j.ceramint.2018.06.137.
- [32] A. Ito, K. Onuma, Growth of hydroxyapatite crystals, Cryst. Growth Technol. Elsevier, 2003, pp. 525–559, https://doi.org/10.1016/B978-081551453-4. 50018-X
- [33] R. Rodríguez-Clemente, A. López-Macipe, J. Gómez-Morales, J. Torrent-Burgués, V.M. Castaño, Hydroxyapatite precipitation: a case of nucleation-aggregation-agglomeration-growth mechanism, J. Eur. Ceram. Soc. 18 (2002) 1351–1356, https:// doi.org/10.1016/s0955-2219(98)00064-8.
- [34] D. Gebauer, A. Völkel, H. Cölfen, Stable prenucleation calcium carbonate clusters, Science 322 (80) (2008) 1819–1822, https://doi.org/10.1126/science.1164271.
- [35] F. Nudelman, K. Pieterse, A. George, P.H.H. Bomans, H. Friedrich, L.J. Brylka, P.A.J. Hilbers, G. De With, N.A.J.M. Sommerdijk, The role of collagen in bone apatite formation in the presence of hydroxyapatite nucleation inhibitors, Nat. Mater. 9 (2010) 1004–1009, https://doi.org/10.1038/nmat2875.
- [36] I. Khattech, M. Jemal, Thermochemistry of phosphate products. Part I: standard enthalpy of formation of tristrontium phosphate and strontium chlorapatite, Thermochim. Acta 298 (1997) 17–21, https://doi.org/10.1016/S0040-6031(97) 00120-2.
- [37] L. Amirouche, M. Plapp, Phase-field modeling of the discontinuous precipitation reaction, Acta Mater. 57 (2009) 237–247, https://doi.org/10.1016/j.actamat.2008. 09 015
- [38] H.K. Henisch, "Growth waves" in periodic precipitation, J. Cryst. Growth 87 (1988) 571–572. https://doi.org/10.1016/0022-0248(88)90107-8
- 571–572, https://doi.org/10.1016/0022-0248(88)90107-8.
  [39] P.S. Braterman, C. Tan, S. Yang, Periodic precipitation in a competitive particle growth model, Mater. Res. Bull. 29 (1994) 287–292, https://doi.org/10.1016/0025-5408(94)90025-6.
- [40] R.W. Balluffi, S.M. Allen, W.C. Carter, Kinetics of Materials, John Wiley & Sons, Inc., Hoboken, NJ, USA, 2005, https://doi.org/10.1002/0471749311.
- [41] G.A. Andreev, M. Hartmanova, Classification of precipitation phenomena in ionic crystals, Mater. Chem. Phys. 10 (1984) 309–315, https://doi.org/10.1016/0254-0584(84)90092-0.
- [42] K. Venkateswarlu, M. Sandhyarani, T.A. Nellaippan, N. Rameshbabu, Estimation of crystallite size, lattice strain and dislocation density of nanocrystalline carbonate substituted hydroxyapatite by X-ray peak variance analysis, Procedia Mater. Sci. 5 (2014) 212–221, https://doi.org/10.1016/j.mspro.2014.07.260.
- [43] Y. Kim, A.S. Schenk, J. Ihli, A.N. Kulak, N.B.J. Hetherington, C.C. Tang, W.W. Schmahl, E. Griesshaber, G. Hyett, F.C. Meldrum, A critical analysis of calcium carbonate mesocrystals, Nat. Commun. 5 (2014) 4341, https://doi.org/10. 1038/ncomms5341
- [44] D. Balzar, Characterization of strains and defects in nanomaterials by diffraction techniques, Model. Charact. Prod. Nanomater. Elsevier, 2015, pp. 145–166, , https://doi.org/10.1016/B978-1-78242-228-0.00005-3.
- [45] J. Zeglinski, M. Nolan, M. Bredol, S.A.M. Tofail, A. Schatte, S.A.M. Tofail, Unravelling the specific site preference in doping of calcium hydroxyapatite with strontium from ab initio investigations and Rietveld analyses, Phys. Chem. Chem. Phys. 14 (2012) 3435–3443, https://doi.org/10.1039/c2cp23163h.